Available online at www.sciencedirect.com

SCIENCE DIRECT®

Marine Chemistry 91 (2004) 101–115

MARINE CHEMISTRY

www.elsevier.com/locate/marchem

Adsorption and precipitation of iron from seawater on a marine bacteriophage (PWH3A-P1)

Christopher J. Daughney[a,*], Xavier Châtellier[b], Amy Chan[c], Paul Kenward[d], Danielle Fortin[e], Curtis A. Suttle[c], David A. Fowle[d]

[a]*Institute of Geological and Nuclear Sciences, P.O. Box 30368, Lower Hutt, New Zealand*
[b]*Géosciences Rennes, Université de Rennes 1, Campus de Beaulieu, Bâtiment 15 F-35042 Rennes cedex, France*
[c]*Department of Earth and Ocean Sciences, University of British Columbia, 6270 University Boulevard, Vancouver, British Columbia, Canada V6T 1Z4*
[d]*Great Lakes Institute for Environmental Research, University of Windsor, 40 Sunset Avenue, Windsor, Ontario, Canada N9B 2P3*
[e]*Department of Earth Sciences, University of Ottawa, 140 Louis Pasteur, Ottawa, Ontario, Canada K1N 6N5*

Received 6 January 2004; received in revised form 27 May 2004; accepted 1 June 2004
Available online 21 August 2004

Abstract

The distribution and chemical form of iron in marine environments is of particular interest to oceanographers because of its effect on primary productivity. The high abundance of viruses in the ocean and their small size suggest that they might serve as nucleation centers for iron adsorption and precipitation in the ocean. Hence, we performed laboratory experiments to quantify the adsorption and precipitation of iron by a marine bacteriophage (PWH3a-P1). Acid–base titrations and zeta potential measurements were performed to determine if the virus interacted with protons, and if so, to determine the type, concentration, and reactivity of functional groups present on the viruses. Iron precipitation experiments were conducted to investigate interactions between iron and the viruses. The titrations and zeta potential measurements were well described by a model considering two types of reactive sites on the viruses, with log K values of −4.44 and −8.18, and a total site concentration of 3.64×10^{-18} mol per virus. High-magnification observations of the viruses in the presence of iron by whole-mount transmission electron microscopy showed evidence of both adsorption and mineral nucleation. The experimental results clearly demonstrate the potential of marine bacteriophage to serve as nuclei for iron adsorption and precipitation, and the models developed from the data suggest that viruses might represent a significant reservoir of iron in seawater. However, these experiments utilized greatly simplified chemistry and a limited range of iron-to-virus concentration ratios relative to natural seawater, and so the results of this study do not prove that viruses affect the marine iron cycle, but rather serve to justify continued research into iron–virus interactions, in the laboratory and in the field.

Keywords: Sea water; Virus; Iron; Adsorption; Precipitation

* Corresponding author. Tel.: +1 64 04 570 4751.
E-mail address: c.daughney@gns.cri.nz (C.J. Daughney).

0304-4203/$ - see front matter © 2004 Elsevier B.V. All rights reserved.
doi:10.1016/j.marchem.2004.06.003

1. Introduction

The geochemical cycling of iron controls rates of primary productivity in vast areas of the ocean. Fertilization experiments have demonstrated that iron addition stimulates primary productivity in the surface waters of the Equatorial Pacific (Coale et al., 1996), the Southern Ocean (Boyd et al., 2000), and even in coastal areas subject to upwelling (Hutchins et al., 1998, 2002). Indeed, it is generally accepted that primary productivity in large areas of the world's oceans is iron limited (Behrenfeld and Kolber, 1999). Through its link to primary productivity, iron plays an important role in the cycling of carbon, nitrogen, and phosphorus in marine environments (Wu et al., 2000). Paleorecords from Antarctic ice show a correlation between iron supply to the oceans and atmospheric CO_2 concentration, suggesting that the link between iron availability and primary productivity has been important for much of the earth's recent history (Martin, 1990; Petit et al., 1999).

Due in part to its relationship to primary productivity, the distribution and chemical form of iron in seawater has been intensely investigated (see review by de Baar and de Jong, 2001 and references therein). Most research on iron cycling in seawater considers the traditional categories of particulate iron and dissolved iron. These categories are typically operationally defined with a 0.2- or 0.45-μm filter membrane. Iron in the particulate phase typically accounts for 50–80% of the total iron, and ranges in concentration from less than 1 nmol l^{-1} in the open ocean to several hundred nmol l^{-1} in coastal waters and near hydrothermal vents. Between 50% and 90% of the particulate iron is in refractory mineral form. The remaining particulate iron is easily solubilized by dilute acid, and is associated with organic and mineral sorbents. In the dissolved phase, concentrations of iron in seawater range from less than 1 nmol l^{-1} in surface waters of the open ocean to as much as 3 mmol l^{-1} in the proximity of seafloor hydrothermal vents and in sediment pore waters of anoxic basins or fjords. Up to 50% of "dissolved iron" (i.e., that which passes a 0.2-μm filter membrane) is actually in the form of colloids between 0.03 and 0.1 μm in diameter (Wells and Goldberg, 1992, 1993, 1994; Wu and Luther, 1994, 1996; Nishioka et al., 2001; Wu et al., 2001). The speciation of this colloidal iron has not been systematically investigated, but it has been suggested that it is largely organically bound (de Baar and de Jong, 2001). The iron that passes a 0.03-μm filter is described as truly dissolved. Between 90% and 99% of truly dissolved iron is believed to be strongly chelated by organic ligands (Rue and Bruland, 1995; Wu and Luther, 1995).

In this investigation, we hypothesize that a fraction of the colloidal iron (i.e., 0.03–0.2-μm diameter) iron might be associated with viruses in the marine environment. Several lines of evidence support this hypothesis. First, viruses are in the right size range, with capsid diameters typically between 50 and 100 nm (by comparison, marine bacterial cell dimensions are usually ca. 0.3–1.5 μm). Second, viruses are abundant in ocean waters. There are typically 10^9–10^{10} virus-like particles per liter, and viral abundances in ocean waters generally exceed those of bacteria by about an order of magnitude (Bergh et al., 1989; Boehme et al., 1993; Maranger and Bird, 1995; Weinbauer and Suttle, 1997; Marie et al., 1999; Culley and Welschmeyer, 2002). Considering both size and abundance, viruses likely represent a small but significant fraction of the microbial surface area in the ocean. Third, previous research indicates that iron is strongly associated with organic and biological materials in seawater. The association of iron with biological particles is supported by several laboratory studies showing that algae and bacteria act as sites for the adsorption and precipitation of dissolved metals, including iron (Warren and Ferris, 1998; Châtellier et al., 2001; Daughney et al., 2001; Fein et al., 2002), and by the direct observation of iron-coated bacteria in seawater (Cowen and Silver, 1984; Tazaki, 1994; Heldal et al., 1996; Fortin et al., 1998). Although iron–virus interactions have not yet been systematically investigated, virus capsids, being composed of protein (Ackerman and DuBow, 1987), potentially display the same types of carboxyl and amino groups that have been implicated in metal binding by bacteria and algae (Shumate and Strandberg, 1985; Plette et al., 1995; Fein et al., 1997; Daughney et al., 1998). Overall, the ubiquity, abundance, and reactivity of viruses suggest that they could serve as nuclei for the adsorption and precipitation of iron in seawater.

Scientific testing of the above hypothesis would ideally involve careful laboratory studies of iron–virus interactions in systems closely resembling natural seawater, coupled with field observations of iron association with marine viruses. For cost efficiency and for comparison to other research projects currently underway in our laboratories, we began by focusing on the laboratory experiments. We performed acid–base titrations and zeta potential measurements with the marine bacteriophage PWH3a-P1 to determine if this virus interacts with protons, and if so, to determine the type, concentration, and reactivity of functional groups involved in these proton–virus interactions. These methods have been applied to bacterial (e.g., Fein et al., 1997; Cox et al., 1999), algal (Xue et al., 1988), and mineral (e.g., Stumm and Morgan, 1981) surfaces, and several studies have shown that the tendency of a surface to interact with protons is correlated to its tendency to interact with dissolved metal ions (Stumm and Morgan, 1981; Langmuir, 1997; Daughney et al., 1998). Iron precipitation experiments were used to investigate interactions between iron and the viruses. In these experiments, iron was precipitated in the presence of the viruses at two different ratios of iron concentration to virus abundance, and whole-mount transmission electron microscopy (TEM) was used to examine the viruses before and after exposure to iron. The overall aim of this investigation was to conduct preliminary laboratory experiments to determine if and to what degree viruses could retain iron in a laboratory setting, to provide justification for future laboratory and field research.

2. Materials and methods

2.1. Preparation of virus suspensions

Bacteriophage PWH3a-P1 and its host *Vibrio* sp. strain PWH3a, an uncharacterized bacterium closely related to *Vibrio natriegens*, were isolated from the coastal waters of the Gulf of Mexico. PWH3a-P1 belongs to the Myoviridae and possesses an icosahedral head with a diameter of ca. 83 nm and a contractile tail ca. 100-nm long (Suttle and Chen, 1992). PWH3a-P1 was selected as a representative marine virus, although we point out that it is not ubiquitous in marine environments.

For these experiments, PWH3a-P1 was amplified on its host using a plate-lysate method (Suttle and Chen, 1992). Briefly, a bacterial colony from a freshly streaked plate was added to liquid broth (peptone, Casamino acids, yeast extract; 0.05% w/v each) and 0.3% v/v glycerol, and cultured overnight at 27 °C. Exponentially growing host cells were combined with infectious viruses and allowed to adsorb for 15 min. Subsamples (0.5 ml) of this mixture were combined with 2.5-ml volumes of nutrient-enriched 0.6% molten agar and poured over 1% agar underlays on 33 separate Petri plates. Upon lysis of the bacterial lawns, the top agar was scraped off the plates and the viruses were eluted in artificial seawater (ESAW) (Harrison et al., 1980) modified by the addition of Selenium (SESAW) or Selenium and TRIS buffer (SESAWT) (Cottrell and Suttle, 1991). Agar particles were removed by slow-speed centrifugation and filtration through a GFF glass-fiber filter (Whatman). The viruses in the filtered lysates were concentrated by ultracentrifugation at ca. 180,000×g for 3 h, and subsequently washed five times by ultracentrifugation and resuspension of the pellets in SESAWT, yielding ca. 10^{14} total viral particles per liter. The washing procedure was intended to remove organic substances and metal ions from the virus capsids. Although we cannot confirm the effectiveness of the washing procedure, similar protocols have been employed to prepare bacterial suspensions for titration and metal-interaction experiments (Fein et al., 1997; Cox et al., 1999).

The amplified stock of PWH3a-P1 in SESAWT was used to create several suspensions (C1–C4), to test the effect of various post-treatments. No preservatives or posttreatments were employed with C1. For C2, the viruses were resuspended in SESAW; no preservatives or postgrowth treatments were used. C3 was unpreserved, and the viral capsids disrupted to release the nucleic acids by freezing at −20 °C for 45 min followed by heating at 75 °C for 5 min. C4 was unpreserved but treated with 5–10 U of RNase-free DNase (Amersham) for 60 min to destroy free DNA. Overall, this produced four virus suspensions, each with a different virus concentration due to the addition of various reagents.

2.2. Zeta potential measurements

Zeta potential measurements were conducted at the Great Lakes Institute for Environmental Research, University of Windsor (Canada). The measurements were used to determine the isoelectric point of PWH3a-P1, and to evaluate the relationship between solution pH and the electric potential of the virus surfaces. Aliquots of the stock solution C2 (see above) were divided into 10 identical polypropylene containers, diluted with 0.5 mol l^{-1} $NaNO_3$ to yield ca. 10^9 viruses l^{-1}, and the pH of each solution was adjusted to a different value using NaOH and/or HNO_3. Following equilibration for 30 min, the pH was measured using a VWR Symphony SR301 meter (Edmonton, Canada), and zeta potential measurements were made using a Malvern Zetasizer 3000 (Malvern, UK).

2.3. Acid–base titrations

Acid–base titrations were used to determine the types, concentrations, and acidity constants for functional groups involved in proton–virus interactions. We performed titrations on PWH3a-P1 from suspensions C1 to C4 diluted with 0.5 mol l^{-1} $NaNO_3$; two different dilutions ratios were performed with C1, and duplicate titrations were performed on independently prepared dilutions of all of the suspensions. Titrations of 0.5 mol l^{-1} $NaNO_3$, diluted SESAW, diluted SESAWT, and diluted SESAWT with DNase were also performed. Following selected titrations, the viruses were removed from suspension by centrifugation (180,000×g for 30 min), and titrations of the supernatant were conducted to quantify the buffering capacity of any dissolved organic compounds that were present in the suspensions.

In all cases, titrations were performed as described by Daughney et al. (2001). A weighed aliquot of the parent suspension containing the viruses was diluted with a known weight (10–30 g) of 0.5 mol l^{-1} $NaNO_3$, resulting in between 1.5×10^{13} and 5.8×10^{13} viruses per liter. The suspension was then placed in an air-tight polystyrene reaction vessel. The pH was adjusted to ca. 3.5 by addition of an aliquot of standardized HNO_3, and the suspension was mixed with a stirrer and bubbled with CO_2-free N_2 gas for 30 min, to purge the suspension of dissolved CO_2. The titrations were conducted in an up-pH direction using a Radiometer TTT85/ABU80 autotitrator (Copenhagen, Denmark) at the Department of Earth Sciences at the University of Ottawa (Canada) or a Metrohm Titrino 736 autotitrator (Herisau, Switzerland) at the Wairakei Research Centre of the Institute of Geological and Nuclear Sciences (New Zealand). Standardized CO_2-free NaOH was used as the titrant, and the suspension was bubbled with CO_2-free N_2 gas over the course of the titration. Following each addition of titrant, the pH of the suspension was recorded when a stability of at least 0.1 mV/s was obtained. At the completion of each titration (pH~10), an aliquot of standardized HNO_3 was added to the titration vessel to return the pH to roughly 3.5, and a second up-pH titration was conducted to evaluate the reversibility of the proton–virus interaction.

2.4. Iron precipitation experiments

To investigate the ability of the viruses to adsorb iron or to serve as nucleation sites for iron precipitation, we oxidized Fe(II) in the presence of the viruses according to the protocol of Châtellier et al. (2001), which had been developed to investigate the reactivity of bacterial surfaces with respect to iron oxidation and precipitation. A suspension of viruses in SESAW was diluted with 10^{-3} mol l^{-1} $NaNO_3$ to yield approximately 24.5 ml of a suspension containing ~7×10^{13} viruses l^{-1}. This suspension was adjusted to pH 7.0±0.1 with standardized NaOH, then equilibrated with the atmosphere by moderate agitation with a magnetic stirrer for 1.5 h. Iron oxides were synthesized by simultaneous dropwise addition of 10^{-2} mol l^{-1} $FeCl_2$ and standardized CO_2-free NaOH. This protocol permitted the pH to be maintained at 7.0±0.1 during the formation of the iron oxides (Châtellier et al., 2001). Two suspensions were prepared, one with a final total iron concentration ($[Fe]_T$) of 2×10^{-4} mol l^{-1}, the other with $[Fe]_T=1\times10^{-3}$ mol l^{-1}. Control experiments were not performed, because abiotic iron oxides formed in sterile solutions with ($[Fe]_T$) of 2×10^{-4} mol l^{-1} are described by Châtellier et al. (2001).

TEM was used to examine particles that had been rinsed with distilled water and left to dry on Formvar-coated copper grids. The grids were first observed with a JEOL JEM 1200EX TEMSCAN microscope operated at 80 kV. EDS spectra were obtained with a 1XRF system and collected live for 60 s. High-

resolution observations were performed with a JEOL 2010F field emission electron microscope. Selected area electron diffraction (SAED) was performed at 200 kV (camera constant=50 cm).

In these iron precipitation experiments, although the total concentrations of iron and of viruses exceeded typical ocean concentrations by about five orders of magnitude, the iron-to-virus ratio was comparable to seawater. For example, the lower of the two $[Fe]_T$ concentrations used in our experiments gave roughly 3×10^{-18} mol Fe per virus, very similar to the ratio expected in natural seawater, where typical $[Fe]_T$ and virus concentrations would be ca. 10^{-9} mol l^{-1} and 10^{9} viruses l^{-1}, respectively. The higher of the two $[Fe]_T$ concentrations used in our experiments gave roughly 10^{-17} mol Fe per virus, which we chose in the attempt to ensure saturation of reactive sites on the viruses (see below). We point out, however, that the higher $[Fe]_T$ used in our experiments still had relevance to certain natural marine environments, such those around hydrothermal vents, where Fe concentrations could exceed those of the open ocean by an order of magnitude.

2.5. Modeling

A modified version of the computer program FITEQL 2.0 (Westall, 1982) was used to construct geochemical models describing proton and iron interactions with the viruses. The modified version, denoted here as FITMOD, permitted simultaneous modeling of systems with different solid-to-solution ratios, and it included a double layer model in which exchange sites were assumed to be uniformly distributed through a Donnan shell volume (Oshima and Kondo, 1991; van der Wal et al., 1997; Wonders et al., 1997; Wasserman and Felmy, 1998; Martinez et al., 2002), rather than concentrated on a plane immediately at the virus–solution interface. The deprotonation reactions of different types of functional groups (L_1H, L_2H, …, L_nH) within the Donnan volume were described by the following general chemical reaction and mass action law:

$$RL_nH^x \leftrightarrow RL_n^{x-1} + H^+$$

$$K_n = \frac{\left[RL_n^{x-1}\right]a_{H^+}}{[RL_nH^x]}$$

where R represents the organic compound to which the functional group L_nH is attached, x represents the charge of the protonated functional group, K_n represents the stability constant describing deprotonation, square brackets represent the concentration of the enclosed functional group (mol l^{-1} solution), and a represents the activity of the subscripted species (mol l^{-1}). Interaction of a metal ion M with a virus functional group was described by the following chemical reaction and mass action law:

$$RL_nH^x + M^y \leftrightarrow RL_nM^{x+y-1} + H^+$$

$$K_n^M = \frac{[RL_nM^{x+y-1}]a_{H^+}}{[RL_nH^x]a_{M^y}}$$

where y represents the charge of the metal ion. These formulations (or very similar ones) have been successfully applied to describe proton and metal interactions with bacteria (Fein et al., 1997; Daughney et al., 1998; Cox et al., 1999; Fowle and Fein, 1999; Martinez et al., 2002), and are analogous to formulations used for mineral surfaces (Stumm and Morgan, 1981; Langmuir, 1997).

For surfaces displaying an electric charge, the interaction between the adsorbing ion and the surface will affect the mass action expression above. This electrostatic interaction was accounted for with the following relationship (Stumm and Morgan, 1981):

$$K_n^{\text{int}} = K_n\exp(-zF\psi/RT)$$

where K_n^{int} represents the (intrinsic) stability constant referenced to the condition of zero surface charge, and z, F, ψ, R, and T refer to the charge of the adsorbing ion, Faraday's constant, the electric potential at the location of adsorption, the gas constant, and the absolute temperature, respectively. The electric potential within the Donnan shell (ψ_D) was calculated as described by Oshima and Kondo (1991):

$$\psi_D = \text{arcsinh}\left(\frac{\rho_D}{2CF}\right)$$

where ρ_D and C represent the charge density within the Donnan shell (C m^{-3}) and the ionic concentration of the bulk electrolyte (mol m^{-3}). The value of ρ_D was determined from the experimental proton adsorption data, the virus concentration, and the thickness of the Donnan shell, and was optimized during the

modeling. The electric potential at the virus–solution interface (ψ_0) and its relationship to ψ_D were calculated as described by Wasserman and Felmy (1998). For the systems investigated here, at depths in excess of 0.2 nm within the capsid, the electric potential was equal to the Donnan potential. In the solution phase, the decay of ψ_0 with distance from the surface was described using the diffuse layer model (Stumm and Morgan, 1981). For our systems, with an ionic strength of 0.5 mol l^{-1}, the thickness of the diffuse portion of the electric double layer was roughly 0.5 nm. For all electric double-layer calculations, the viruses were assumed to have a specific surface area of 48 m^2 g^{-1}, based on an average diameter of 83 nm (Suttle and Chen, 1992) and a buoyant density of 1.5 g cm^{-3} (Ackerman and DuBow, 1987). As a first approximation, the virus capsids were assumed to have a Donnan thickness of 15 nm and a dielectric constant of 60 (van der Wal et al., 1997), although these parameters were varied over a reasonable range during the modeling.

In addition to the formulations for proton and metal interaction with the viruses as described above, all models constructed in this investigation bore certain standard features. All stability constants were adjusted for ionic strength using the Davies equation (Langmuir, 1997), and all values tabulated in this report were referenced to zero ionic strength (as well as zero electric potential). Equilibria describing iron hydrolysis and the deprotonation of water, the acid, the base, and the electrolyte were included in the models, with stability constants taken from Smith and Martell (1976). All stability constants were referenced to 25 °C.

The computer program FITMOD was used to compare the fit of each geochemical model to the experimental data. Like FITEQL, FITMOD calculates the error (Y) in the chemical mass balance equation, so that the overall variance $V(Y)$ provides a quantitative measure of goodness-of-fit (Westall, 1982). For systems containing a reactive surface, values of $V(Y)$ between 1 and 20 indicate an acceptable fit to the data.

3. Results and discussion

3.1. Zeta potential measurements

The relationship between the zeta potential of PWH3a-P1 and pH (Fig. 1) was similar to the previously reported results for viruses (Ryan et al., 1999) and other biological surfaces (van Loosdrecht

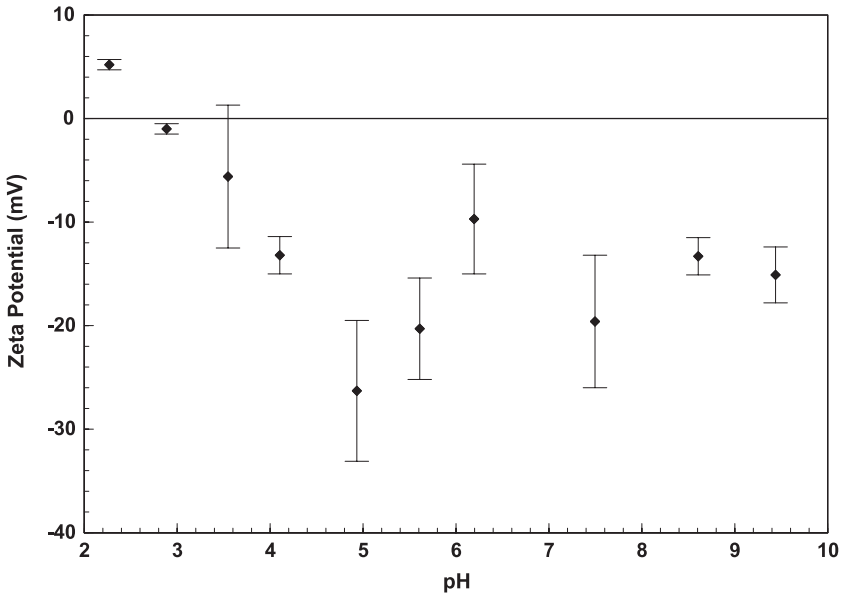

Fig. 1. Zeta potential of viruses (culture C2) in 0.5 mol l^{-1} $NaNO_3$ as a function of pH. Error bars represent two standard deviations from the mean.

et al., 1987; Collins and Stotzky, 1992; Campbell et al., 1997). The error bars in Fig. 1 represent two standard deviations from the mean, and pertain to variations in zeta potential observed within a single sample. Variability of this magnitude has been observed for other biological colloids (Campbell et al., 1997), and is expected for most types of colloids due to effects such as particle heterogeneity, aggregation, sedimentation, and Brownian motion (Hunter, 2002; Oshima, 2002). The isoelectric point of the virus was found to be approximately 3.0, similar to several other virus species, but on the lower end of the range of results previously reported in the literature (Gerba, 1984).

The zeta potential data could be used to conceptualize the proton–virus interactions. The data indicated that the virus surfaces accumulated a negative surface charge with increasing pH. This provided evidence of the existence of anionic functional groups, and of the deprotonation of these groups with increasing pH. The structure of these anionic functional groups could not be determined from the available data, but the transition from positive to negative zeta potential within the range 2<pH<4 suggested that carboxyl structures may have been important. The fact that the zeta potential was positive at the most acidic pH provided evidence of the existence of cationic functional groups, which could be amino groups. Carboxyl and amino functional groups are likely to exist, given the proteinaceous composition of viral capsids (Gerba, 1984). Furthermore, carboxyl and amino functional groups have been assumed responsible for the zeta potential vs. pH relationship observed for bacterial surfaces (Busscher et al., 2000), and these types of sites have been implicated in proton binding by bacteria and algae (Shumate and Strandberg, 1985; Plette et al., 1995; Fein et al., 1997; Daughney et al., 1998; Cox et al., 1999; Martinez et al., 2002). We stress that the available data do not permit us to determine if proton-active functional groups were components of the virus capsids, or were related to surface-bound organic substances that were not removed from the capsids during the washing procedure. To quantify the concentrations of these functional groups and their reactivity toward protons, we performed acid–base titrations, as discussed below.

3.2. Acid–base titrations

Titrations of 0.5 mol l^{-1} $NaNO_3$ were in good agreement with theoretical predictions, indicating that that the experimental apparatus did not interact with protons and that CO_2 contamination was minimal. Titrations of 1% or 2% SESAW or SESAWT in 0.5 mol l^{-1} $NaNO_3$ were also in good agreement with theoretical predictions. The results indicted that TRIS, when present, imparted a significant buffering capacity to the solution, but the components of SESAW did not. To account for the effect of the TRIS, a model was constructed using log K_{TRIS} for deprotonation=−8.2 (Martell and Smith, 1977), and the accuracy of the model was assessed by comparing observed buffering capacity in virus-free solutions to the quantity of TRIS over a range of concentrations. Titrations of the DNase enzyme in 0.5 mol l^{-1} $NaNO_3$ were very similar to those of 0.5 mol l^{-1} $NaNO_3$ alone, indicating that the enzyme did not interact with protons or the experimental apparatus.

The titration data for the virus suspensions (Fig. 2) showed excellent agreement between the first and second up-pH titrations for each suspension, and between duplicate titrations of independently prepared dilutions of the parent stock, although for clarity only one titration from each data set is plotted. As well, to compare among experiments, if the suspension contained TRIS, its effect has been subtracted from the curves in Fig. 2 using the model described above.

The experimental data indicated that the viruses imparted a measurable buffering capacity to the suspension, relative to the background electrolyte, and that the degree of buffering increased with virus concentration. In all cases, titrations of solutions from which the viruses had been removed were very similar to titrations of the background electrolyte, suggesting that any compounds released by the viruses were not present in significant concentrations or did not interact with protons. The replicate titrations indicated that the proton–virus interactions were rapid, reversible, and reproducible, suggesting that the observed buffering was caused by proton adsorption–desorption reactions, rather than by irreversible chemical reactions. The reproducibility and reversibility of the titrations also suggests that artifacts related to incomplete removal of metal ions from the virus capsids during rinsing were probably minimal. Further evidence for

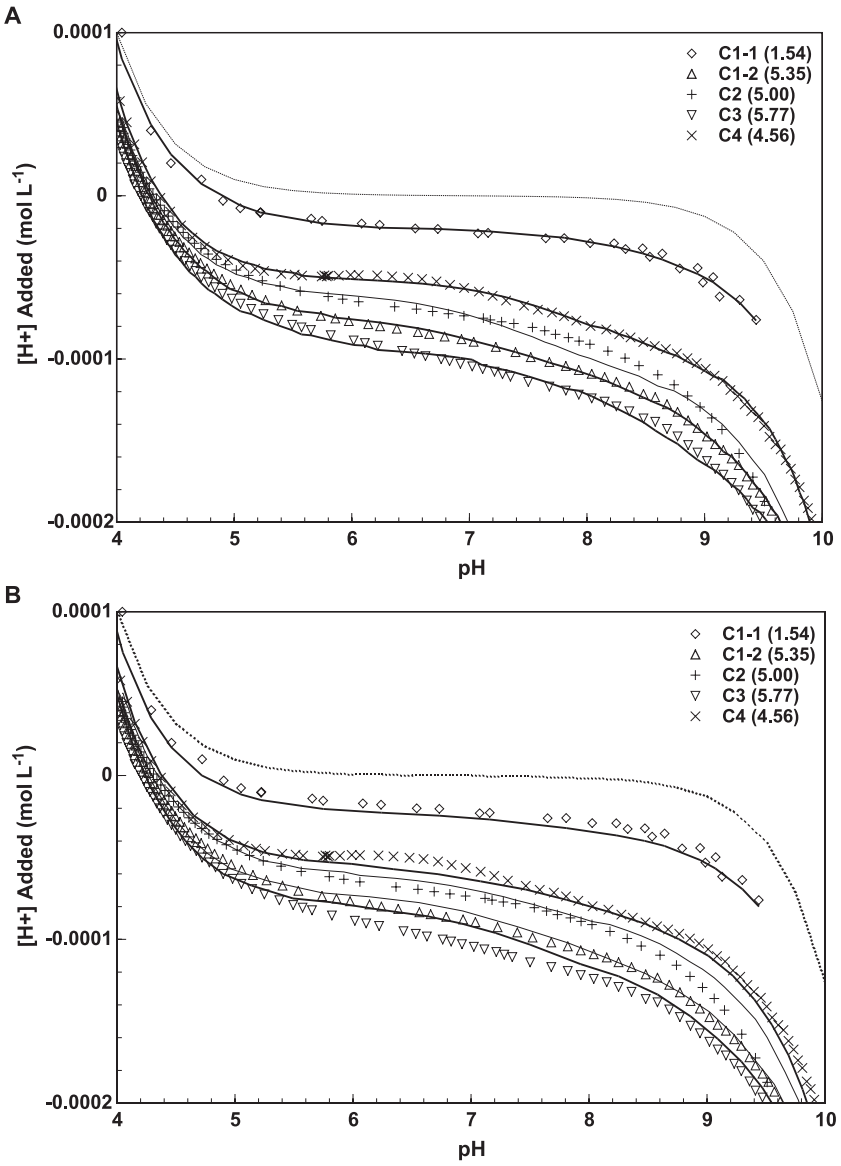

Fig. 2. Net concentration of protons added during acid–base titration of suspensions containing viruses in 0.5 mol l^{-1} $NaNO_3$ electrolyte, as a function of solution pH. Scatter points represent experimental data for different cultures, with virus concentration given in parentheses ($\times 10^{13}$ viruses l^{-1}). Dotted line represents theoretical prediction for titration of the electrolyte alone. (A) Solid lines represent best-fitting models for each individual data set, with parameters as given in Table 1. (B) Solid lines represent the fit of the single model that best describes all of the data from each of the individual data sets (Model 'All', Table 1).

the latter comes from Fein et al. (1997) and Daughney et al. (2001), who show that an acid-rinse step has little effect on the titration data for the bacterium *Bacillus subtilis*.

Slight variations in the shape of the titration curves suggested that the various treatment methods may have caused small changes in the buffering capacity of the suspensions. For example, the suspension containing the heat-treated viruses (C3) was unique, in that it showed a more negative slope in buffering capacity above pH 8 than any other suspension. This may have been because the heat disruption exposed or

otherwise increased the concentration of functional groups capable of interacting with protons at pH>8. The suspension that had been treated with DNase (Stock C4) displayed a slightly more negative slope than other titration curves in the range 6<pH<8. This implied that digestion of free DNA exposed or increased the concentration of exchange sites capable of interacting with protons over this pH range. Despite these slight variations, for the majority of data sets, the titration curves were generally similar, suggesting that the major differences in buffering were related to the concentration of viruses present.

Using FITMOD, we modeled each of the titration data sets individually. Models considering only one type of functional group produced values of $V(Y)$ much greater than 20, indicating a poor fit to the experimental data (Westall, 1982). Models considering two distinct types of reactive sites (one anionic, one cationic) provided good fits to the experimental data (Fig. 2A, Table 1) and produced low values of $V(Y)$, indicating the two-site models provided sufficient complexity to describe the data.

The FITMOD models for the individual titration data sets were used to identify the types of structures responsible for the observed buffering. For all two-site models, the values of the deprotonation constants for each distinct type of site were quite similar (Table 1). Based on the magnitudes of these deprotonation constants relative to those of short-chain organic acids (Martell and Smith, 1977), and taking the conceptual model developed from the zeta potential data into account, we conclude that these sites represent carboxyl ($R\text{-}COOH^0$) and amino ($R\text{-}NH_3^+$) structures. The existence of these types of functional groups was supported by the zeta potential data (see above), and such functional groups have been implicated in proton interactions with bacteria (Fein et al., 1997; Daughney et al., 1998; Cox et al., 1999; Daughney et al., 2001; Martinez et al., 2002).

Table 1
Parameters for models describing proton–virus interactions

Susp[a]	Carboxyl[b]		Aminob		Variance[c]	
	log K[d]	C[e]	log K	C	$V(Y)_1$	$V(Y)_2$
C1-1	−5.82	1.34	−9.51	2.90	6.6	10.0
C1-2	−4.48	1.50	−8.03	2.07	1.3	37.8
C2	−4.55	1.25	−8.40	2.24	14.2	24.8
C3	−4.36	1.76	−7.49	1.50	3.4	74.6
C4	−4.59	1.38	−8.78	2.50	2.1	7.2
All[f]	−4.44	1.47	−8.18	2.17	–	9.6

[a] Suspension used for the titration; note that titrations at two different dilutions were performed with suspension C1.

[b] All models consider carboxyl sites of the form $R\text{-}COOH^0$ and amino sites of the form $R\text{-}NH_3^+$ uniformly distributed through a Donnan volume with a thickness of 15 nm and an outer diameter of 83 nm.

[c] Variance calculated by FITMOD. $V(Y)_1$ is for the best-fitting model for the individual stock suspension (Fig. 2A), $V(Y)_2$ is the fit of the 'All' model to the each of the individual data sets (Fig. 2B).

[d] Logarithm of the stability constant describing deprotonation, referenced to zero ionic strength and zero electric potential.

[e] Site concentration ($\times 10^{-18}$ mol per virus).

[f] Single best-fitting model for all titration data, except for data from C2d (heat-treated viruses).

The FITMOD models for the individual titration data sets also revealed a relationship between the concentration of viruses and the concentrations of functional groups responsible for buffering (Table 1). To illustrate this relationship, we normalized the total concentration of functional groups in each system (mol l^{-1}) with respect to the number of viruses present (viruses l^{-1}). Normalized in this manner, the calculated total concentration of functional groups varied over a very small range, from 3.26×10^{-18} to 4.24×10^{-18} mol of sites per virus (Table 1). As stated above, we stress that the available data do not permit us to determine if the proton-active functional groups were components of the virus capsids, or were related to surface-bound organic substances that were not removed from the capsids during the washing procedure, or a combination of both.

The calculated concentration of functional groups per virus provided support for the use of the Donnan shell electrostatic model, as opposed to models considering all exchange sites to be situated immediately at the virus–solution interface. If each virus had a surface area of ca. 21,600 nm^2 (based on a radius of 83 nm), then the calculated average site density (ca. 100 sites nm^{-2}) would exceed that of most other geological and organic sorbents by one to two orders of magnitude (Langmuir, 1997). In contrast, if the sites were distributed over a volume ca. 15-nm thick, the average calculated site density would be ca. 10 sites nm^{-3}. This calculated site density would suggest an average volume of 0.1 nm^3 per site, corresponding to a sphere with a radius of ca. 0.3 nm, on the order expected for a binding site on an amino acid (e.g., oxygen, 0.14 nm; nitrogen, 0.13 nm; Faure, 1998).

Furthermore, the surface electric potential (ψ_0) calculated from the Donnan shell model varied from 20 to −30 mV from pH 2 to 10, in reasonable agreement with the zeta potential data. By contrast, the electric potential at the virus–solution interface, as calculated with a constant capacitance model (Stumm and Morgan, 1981), produced an unrealistic result of several volts.

Due to the observed constancy of deprotonation constants and functional group density for the models of the individual titration data sets, we used FITMOD to develop a single model for all of the data (with the exception of the data from the heat-treated virus suspensions C3). The best-fitting two-site model had log K values for carboxyl and amino sites of −4.44 and −8.18, respectively, and a total site concentration of 3.64×10^{-18} mol per virus (9.9 sites nm^{-3}, assuming a 15-nm Donnan shell) (Table 1). This model was of sufficiently low variance to suggest an adequate fit to the data. Having identified that a single set of log K values and site concentrations could provide a reasonable fit to all of the experimental data, we investigated the effect of changing the thickness of the Donnan shell. The best-fitting model parameters and overall $V(Y)$ were insensitive to the Donnan thickness in the range 10–20 nm. Values of Donnan thickness less than 10 nm increased $V(Y)$ and resulted in unrealistically high values of the surface potential ψ_0. Values of the Donnan potential greater than 20 nm also increased $V(Y)$, generally due to a poorer fit to the data in the mid-pH region. Although we did not have a means of directly measuring the thickness of the Donnan shell, the modeling suggested that a value of 15 nm provided a reasonable description of the titration data.

The prediction of the best-fitting two-site model was then compared to each of the individual titration data sets (Fig. 2B, Table 1). In general, the model provided a reasonable fit to the data. This single best-fitting model predicted an increasingly negative surface potential with increasing pH, and in this regard, the titration data and the zeta potential data were not in agreement. It is possible that at the higher pHs, the condensation of counter-ions becomes increasingly important, thus preventing the zeta potential from decreasing below −30 mV, but this hypothesis could not be tested with the available data. Because the parameters of this single best-fitting two-site model matched most of the titration data reasonably well, it was used to interpret the iron precipitation experiments.

3.3. Iron precipitation experiments

In the low Fe systems ($[Fe]_T=2\times10^{-4}$ mol l^{-1}), the viruses were easily identified by TEM as electron-dense individual particles (Fig. 3A). The virus tails were not visible (i.e., they were not electron dense), suggesting that they did not display functional groups

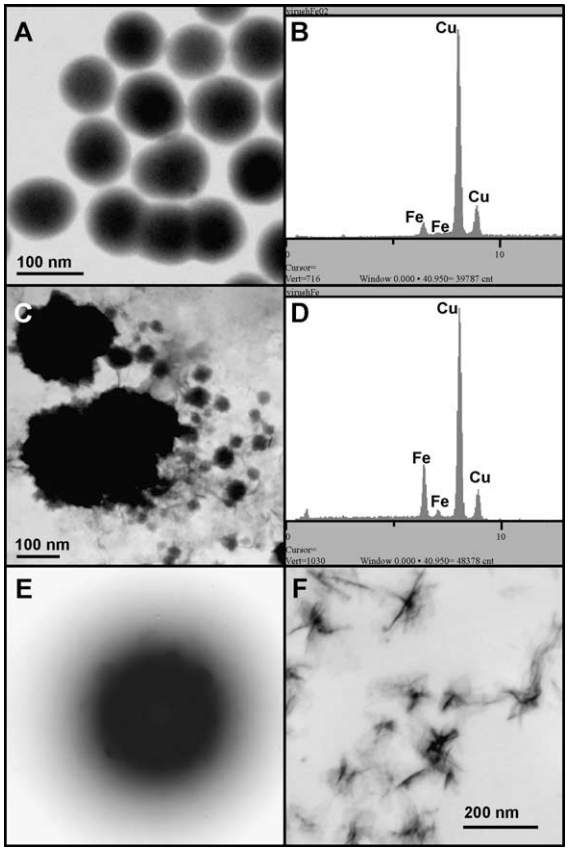

Fig. 3. TEM and EDS observations of viruses in the presence of iron. (A) TEM image of viruses in the presence of $[Fe]_T=2\times10^{-4}$ mol l^{-1}. (B) EDS spectrum corresponding to image A (Cu peaks are from the grid). (C) TEM image of viruses in the presence of $[Fe]_T=1\times10^{-3}$ mol l^{-1}. (D) EDS spectrum corresponding to image C (Cu peaks are from the grid). (E) Selected area electron diffraction pattern of an individual Fe-oxide needle shown in C. (F) TEM image of iron oxide (identified as lepidocrocite) formed in an abiotic system with $[Fe]_T=2\times10^{-4}$ mol l^{-1} using the same experimental protocol (Châtellier et al., 2001).

capable of binding iron. The average apparent diameter of the virus capsids was close to the expected value of 83 nm (Suttle and Chen, 1992). EDS analyses revealed that the capsids were Fe-rich (Fig. 3B), but Fe-oxide precipitates were not visible on their surfaces at the scale of observation. The two peaks for iron in Fig. 3B correspond to the K-alpha and K-beta transitions.

The high Fe systems ($[Fe]_T=1\times10^{-3}$ mol l^{-1}) contained particles of various sizes, ranging from 50 to 300 nm in diameter (Fig. 3C). High-magnification TEM observations revealed that the larger electron-dense particles were composed of clumps of viruses and Fe-oxides, whereas the smaller electron-dense particles corresponded to small aggregates of iron oxide. Again, virus tails were not identifiable (electron dense), implying that they did not interact with iron. Large quantities of Fe-oxides, occurring as thin laths (or needle-like morphology if viewed edge-on) with an average length of 50 nm, were also present, both on the virus surfaces and in the bulk solution (Fig. 3C). EDS analysis of the small and large particles indicated that they were all Fe-rich (Fig. 3D). Again, two iron peaks are visible in the EDS spectrum (Fig. 3D), corresponding to the K-alpha and K-beta transitions. HR-TEM observations of the fine needles present on the viruses first showed that they were all oriented lengthwise on the TEM grid, making it impossible to analyze several orientations of the crystals. The crystals were also very sensitive to the high-intensity electron beam and were rapidly damaged. As a result, few SAED patterns were recorded (Fig. 3E). However, *d*-spacing values corresponding to 1.394, 1.475, and 1.568 Å were measured for some individual needles. These *d*-spacings are common to both lepidocrocite and goethite. Given the limited number of reflections (caused by the tendency of the crystals to align on the grid), it was not possible to determine the mineralogical composition of the Fe-oxide particles. However, Fe-oxides formed in the same way but in the absence of microorganisms were seen to have similar morphology, and could be identified as lepidocrocite (Châtellier et al., 2001; Fig. 3F).

The biomineralization experiments suggested that dissolved iron ions, like protons, were able to penetrate the virus capsids and bind to internal sites. To illustrate, a suspension with roughly 7×10^{13} viruses l^{-1} would have contained a total binding site concentration of roughly 2.5×10^{-4} mol l^{-1} (assuming a binding site density of 3.6×10^{-18} mol per virus). If the sites were uniformly distributed through a Donnan shell 15-nm thick, then roughly 2.4×10^{-5} mol l^{-1} would have been within ca. 1 nm of the capsid surface. Thus, in the biomineralization experiments with $[Fe]_T=2\times10^{-4}$ mol l^{-1}, we added many more Fe atoms than there would have been binding sites within the first nanometer of the capsid surface. However, Fe-oxide precipitation was not apparent. Instead, the viruses appeared as individual electron-dense particles. This implied that the iron penetrated the virus capsids and that a sufficient concentration of iron-binding sites was present to prevent the precipitation of an iron-bearing mineral. In comparison, in the biomineralization experiments with $[Fe]_T=1\times10^{-3}$ mol l^{-1}, iron precipitates were visible on the virus surfaces, suggesting that the capacity of the viruses to adsorb iron had been exceeded, leading to surface precipitation of the mineral and aggregation of the viruses into larger clumps of particles.

4. Discussion and conclusions

The results of this laboratory investigation demonstrate that viruses have capsids that are reactive toward dissolved protons and iron, and that virus capsids can also serve as nuclei for the growth of iron-oxide particles. The reactive sites are likely carboxyl and amino functional groups, with p*K* values of about 4.4 and 8.2, as estimated by acid–base titrations. We have estimated that the total number of proton-reactive sites is on the order of 3.6×10^{-18} mol per virus. Some fraction of these sites may be related to surface-bound organic substances that were not removed from the capsids during the washing procedure. Nonetheless, the magnitude of the calculated site concentration strongly suggests that the proton-reactive sites are distributed throughout the capsid, rather than just immediately at the capsid–solution interface. Our experimental results also show that Fe atoms can penetrate the virus capsids and bind to reactive sites. In the iron precipitation experiment with the low concentration of iron, 2×10^{-4} mol of Fe were added, for an estimated number of 2.5×10^{-4} mol of proton-binding sites, and no precipitation was observed, even though the viruses were clearly

electron-dense. In the experiment with the higher concentration of iron, we added four times as much iron as there were proton-binding sites, and the absorption capacity of the viruses was exceeded, resulting in a heavy Fe-oxide precipitation outside of the viruses. Hence, our study suggests that the number of reactive sites for the Fe atoms is likely quite similar to the number of proton-reactive sites, i.e., about 3.6×10^{-18} mol per virus.

We stress that our results pertain to laboratory systems with simple chemistry and a limited range of iron-to-virus concentration ratios, and so cannot be quantitatively extended to predict the role of viruses on the natural marine iron cycle. For example, it is important to recognize that natural virus communities will be composed of several species, each of which might interact with iron differently. Furthermore, organic coatings on virus capsids might also change their affinity for iron. Other substrates such as dissolved organic ligands might compete with the viruses for the available iron, and other dissolved elements might compete with iron for the binding sites on the viruses. Although our laboratory experiments were performed with iron-to-virus ratios that approximate natural seawater, the iron concentrations were many orders of magnitude above natural levels, and so we cannot assume the same type of iron–virus interactions would occur in nature.

Despite the fact that our results cannot be directly extrapolated to natural seawater, they demonstrate the need for further research on the potential role of viruses in the cycling of iron in ocean waters. To illustrate, consider that seawater typically contains 10^9 to 10^{10} viral-like particles per liter. Our investigation suggests that each virus could absorb about 3–4×10^{-18} mol of iron without loosing its morphologic characteristics, so that about 3–40 nmol l^{-1} of iron could be immobilized by such particles. This is equal to or higher than the total concentration of iron in many parts of the world's oceans. This suggests that viruses could account for a relatively large reservoir of marine iron, and importantly, viruses could bind this concentration of iron and remain in the colloidal size fraction. On the other hand, if more iron accumulates onto viruses, it is likely to exceed the binding site capacity, precipitate as an oxide, and ultimately lead to the formation of virus-oxide aggregates that will fall in the particulate fraction.

The need for further research into the potential role of viruses in the natural marine iron cycle is also supported by other investigations. For example, in a study of iron distribution along a northeast Pacific transect, Nishioka et al. (2001) reported that the <200 kDa (truly dissolved) fraction typically contained 40–65% of the total acid-labile Fe below 200-m depth, whereas the 200 kDa–0.1 μm fraction (which would include viruses) contained 20–30% of the total iron. If this distribution is typical of other locations, then size fraction containing viruses likely represents a significant reservoir of marine iron. Rue and Bruland (1995) reported conditional iron binding constants on the order of 10^{13} for organic ligands in the <0.2-μm fraction. Iron binding constants for bacterial functional groups, expressed in the same stoichiometry, are ca. 10^8–10^{10} (Warren and Ferris, 1998; Daughney et al., 2001). However, a direct comparison of these iron-binding constants is not possible, because they were determined with different methods under different experimental conditions. In addition, the binding affinity of the reactive sites of the viruses could be larger than that of the reactive sites in bacteria. In bacteria, usually only a fraction of the proton-binding sites are reactive toward Fe or other metallic cations (Châtellier and Fortin, submitted for publication; Kulczycki et al., 2002), whereas we have shown here that all the proton-binding sites for the viruses also seem to be iron-binding sites.

Further research may also show that the effect of viruses on marine geochemical cycling is much more extensive than implied above. For example, several studies indicate that the bacterial functional groups responsible for iron chelation can also sequester many other dissolved metals (Fein et al., 1997; Daughney et al., 1998; Fowle and Fein, 1999; Yee and Fein, 2001). If the functional groups on viruses are similar, then they might act as sites for adsorption and nucleation of a variety of elements besides iron, and so they might affect the cycling of metals in a general sense. Further, the effect of viruses on the marine iron cycle may not be limited to adsorption and precipitation. For example, up to 25% of primary production has been estimated to flow through a viral mediated shunt (Wilhelm and Suttle, 1999), as a result of microbial mortality imposed by viral lysis (reviewed in Suttle, 1994, Fuhrman, 1999; Wommack and Colwell, 2000). These potentially important effects emphasize the

need for further research to quantify the role of viruses in the geochemical cycling of metals in the marine environment.

Acknowledgements

We thank Marshall Muller and Moya Appleby for assistance at the Wairakei Research Centre of the Institute of Geological and Nuclear Sciences (New Zealand). We also thank M. West and F. Pearson of McMaster University, Canada, for helping with the TEM and HR-TEM observations.

This research was partially funded by Natural Sciences and Engineering Research Council of Canada grants to D. Fortin and C. Suttle. C. Daughney thanks NSERC for postdoctoral support at the University of Ottawa (Canada).

This paper was greatly improved by the comments of two anonymous reviewers.

Associate editor: Dr. George W. Luther III.

References

Ackerman, H.W., DuBow, M., 1987. Viruses of Prokaryotes. I: General Properties of Bacteriophages. CRC Press, Boca Raton, FL.

Behrenfeld, M.J., Kolber, Z.S., 1999. Widespread iron limitation of phytoplankton in the South Pacific Ocean. Science 283, 840–843.

Bergh, O., Børsheim, K.Y., Bratbak, G., Heldal, M., 1989. High abundance of viruses found in aquatic environments. Nature 340, 467–468.

Boehme, J., Frischer, M.E., Jiang, S.C., Kellogg, Pichard, S., Rose, J.B., Steinway, C., Paul, J.H., 1993. Viruses, bacterioplankton, and phytoplankton in the southeastern Gulf of Mexico: distribution and contribution to oceanic DNA pools. Mar. Ecol., Prog. Ser. 97, 1–10.

Boyd, P.W., et al., 2000. A mesoscale phytoplankton bloom in the polar Southern Ocean stimulated by iron fertilization. Nature 407, 695–702.

Busscher, H.J., Bos, R., van der Mei, H.C., Handley, P.S., 2000. Physicochemistry of microbial adhesion from an overall approach to the limits. In: Baszkin, A., Norde, W. (Eds.), Physical Chemistry of Biological Interfaces. Marcel Dekker, New York, NY, pp. 431–458.

Campbell, P.G.C., Twiss, M.R., Wilkinson, K.J., 1997. Accumulation of natural organic matter on the surfaces of living cells: implications for the interaction of toxic solutes with aquatic biota. Can. J. Fish. Aquat. Sci. 54, 2543–2554.

Châtellier, X., Fortin, D., 2004. Adsorption of ferrous ions onto *Bacillus subtilis* cells. Chem. Geol. (submitted for publication).

Châtellier, X., Fortin, D., West, M.M., Leppard, G.G., Ferris, F.G., 2001. Effect of the presence of bacterial surfaces during the synthesis of Fe oxides by oxidation of ferrous ions. Eur. J. Mineral. 13, 705–714.

Châtellier, X., West, M.M., Rose, J., Fortin, D., Leppard, G.G., Ferris, F.G., 2004. Characterization of iron-oxides formed by the oxidation of ferrous irons in the presence of various bacterial species and inorganic ligands. Geomicrobiol. J. 21, 99–112.

Coale, K.H., et al., 1996. A massive phytoplankton bloom induced by ecosystem-scale iron fertilization experiment in the equatorial Pacific Ocean. Nature 383, 495–501.

Collins, Y.E., Stotzky, G., 1992. Heavy metals alter the electrokinetic properties of bacteria, yeasts and clay minerals. Appl. Envrion. Microbiol. 58, 1592–1600.

Cottrell, M.T., Suttle, C.A., 1991. Widespread occurrence and clonal variation in viruses which cause lysis of a cosmopolitan, eukaryotic marine phytoplankton, *Micromonas pusilla*. Mar. Ecol.. Progr. Ser. 78, 1–9.

Cowen, J.P., Silver, M.W., 1984. The association of iron and manganese with bacteria on marine macroparticulate material. Science 224, 1340–1342.

Cox, J.S., Smith, D.S., Warren, L.A., Ferris, F.G., 1999. Characterizing heterogenous bacterial surface functional groups using discrete affinity spectra for proton binding. Environ. Sci. Technol. 33, 4514–4521.

Culley, A.I., Welschmeyer, N.A., 2002. The abundance, distribution, and correlation of viruses, phytoplankton, and prokaryotes along a Pacific Ocean transect. Limnol. Oceanogr. 47, 1508–1513.

Daughney, C.J., Fein, J.B., Yee, N., 1998. A comparison of the thermodynamics of metal adsorption onto two common bacteria. Chem. Geol. 144, 161–176.

Daughney, C.J., Fowle, D.A., Fortin, D., 2001. The effect of growth phase on proton and metal adsorption by *Bacillus subtilis*. Geochim. Cosmochim. Acta 65, 1025–1035.

de Baar, H.J.W., de Jong, J.T.M., 2001. Distributions, sources and sinks of iron in seawater. In: Turner, D.R., Hunter, K.A. (Eds.), The Biogeochemistry of Iron in Seawater. Wiley, New York, NY, pp. 123–254.

Faure, G., 1998. Principles and Applications of Geochemistry. Prentice-Hall, Upper Saddle River, NJ.

Fein, J.B., Daughney, C.J., Yee, N., Davis, T.A., 1997. A chemical equilibrium model for metal adsorption onto bacterial surfaces. Geochim. Cosmochim. Acta 61, 3319–3328.

Fein, J.B., Scott, S., Rivera, N., 2002. The effect of Fe(III) on Si adsorption by *Bacillus subtilis* cell walls: insights into non-metabolic bacterial precipitation of silicate minerals. Chem. Geol. 182, 265–273.

Fortin, D., Ferris, F.G., Scott, S.D., 1998. Formation of Fe-silicates and Fe-oxides on bacterial surfaces in samples collected near hydrothermal vents on the Southern Explorer Ridge in the northeast Pacific Ocean. Am. Mineral. 83, 1399–1408.

Fowle, D.A., Fein, J.B., 1999. Competitive adsorption of metal cations onto two gram positive bacteria: testing the

chemical equilibrium model. Geochim. Cosmochim. Acta 63, 3059–3067.
Fuhrman, J.A., 1999. Marine viruses and their biogeochemical and ecological effects. Nature 399, 541–548.
Gerba, C.P., 1984. Applied and theoretical aspects of virus adsorption to surfaces. Adv. Appl. Microbiol. 30, 133–168.
Harrison, P.J., Waters, R., Taylor, F.J.R., 1980. A broad spectrum artificial seawater medium for coastal and open ocean phytoplankton. J. Phycol. 16, 28–35.
Heldal, M., Faggerbakke, F.M., Tuomi, P., Bratbak, G., 1996. Abundant populations of iron and manganese sequestering bacteria in coastal water. Aquat. Microb. Ecol. 11, 127–133.
Hunter, R.J., 2002. Electrokinetics of particles. In: Hubbard, A.T., Somasundran, P. (Eds.), Encyclopedia of Surface and Colloid Science. Marcel Dekker, New York, NY, pp. 1907–1919.
Hutchins, D.A., Ditullio, G.R., Zhang, Y., Bruland, K.W., 1998. An iron limitation mosaic in the California upwelling regime. Limnol. Oceanogr. 43, 1037–1054.
Hutchins, D.A., Hare, C.E., Weaver, R.S., Zhang, Y., Firme, G.F., Ditullio, G.R., Alm, M.B., Riseman, S.F., Maucher, J.M., Geesey, M.E., Trick, C.G., Smith, G.J., Rue, E.L., Conn, J., Bruland, K.W., 2002. Phytoplankton iron limitation in the Humboldt current and Peru upwelling. Limnol. Oceanogr. 47, 997–1011.
Kulczycki, E., Ferris, F.G., Fortin, D., 2002. Impact of cell wall structure on the behavior of bacterial cells as sorbents of cadmium and lead. Geomicrobiol. J. 19, 553–565.
Langmuir, D., 1997. Aqueous Environmental Geochemistry. Prentice Hall, Upper Saddle River, NJ.
Maranger, R., Bird, D.F., 1995. Viral abundance in aquatic systems: a comparison between marine and freshwaters. Mar. Ecol., Prog. Ser. 121, 217–226.
Marie, D., Brussaard, C.P.D., Thyrhaug, R., Bratbak, G., Vaulot, D., 1999. Enumeration of marine viruses in culture and natural samples by flow cytometry. Appl. Environ. Microbiol. 65, 45–52.
Martell, A.E., Smith, R.M., 1977. Critical Stability Constants. III: Other organic ligands. Plenum, New York, NY.
Martin, J.H., 1990. Glacial–interglacial CO_2 change: the iron hypothesis. Paleoceanography 5, 1–13.
Martinez, R.E., Smith, D.S., Kulcycki, E., Ferris, F.G., 2002. Determination of intrinsic bacterial surface acidity constants using a Donnan shell model and a continuous pK_a distribution method. J. Colloid Interface Sci. 253, 130–139.
Nishioka, J., Takeda, S., Wong, C.S., Johnson, W.K., 2001. Size-fractioned iron concentrations in the northeast Pacific Ocean: distribution of soluble and small colloidal iron. Mar. Chem. 74, 157–179.
Oshima, H., 2002. Electrokinetic behaviour of particles: theory. In: Hubbard, A.T., Somasundran, P. (Eds.), Encyclopedia of Surface and Colloid Science. Marcel Dekker, New York, NY, pp. 1834–1852.
Oshima, H., Kondo, T., 1991. On the electrophoretic mobility of biological cells. Biophys. Chemist. 39, 191–198.
Petit, J.R., et al., 1999. Climate and atmospheric history of the past 420,000 years from the Vostok ice core, Antarctica. Nature 399, 429–436.
Plette, A.C.C., van Riemsdijk, W.H., Benedetti, M.F., van der Wal, A., 1995. pH dependent charging behaviour of isolated cell walls of a gram-positive soil bacterium. J. Colloid Interface Sci. 173, 354–363.
Rue, E.L., Bruland, K.W., 1995. Complexation of iron(III) by natural organic ligands in the central North Pacific as determined by a new competitive ligand equilibrium/adsorptive stripping voltammmetric method. Mar. Chem. 50, 117–138.
Ryan, J.N., Elimelech, M., Ard, R.A., Harvey, R.W., Johnson, P.R., 1999. Bacteriophage PRD1 and silica colloid transport and recovery in an iron oxide-coated sand aquifer. Environ. Sci. Technol. 33, 63–73.
Shumate II, S.E., Strandberg, G.W., 1985. Accumulation of metals by microbial cells. In: Moo-Young, M. (Ed.), Comprehensive Biotechnology: The Principles, Applications and Regulations of Biotechnology in Industry, Agriculture and Medicine. Elsevier, Amsterdam, pp. 235–247.
Smith, R.M., Martell, A.E., 1976. Critical Stability Constants. IV: Inorganic Complexes. Plenum, New York, NY.
Stumm, W., Morgan, J.J., 1981. Aquatic Chemistry. (2nd ed.)Wiley, New York, NY.
Suttle, C.A., 1994. The significance of viruses to mortality in aquatic microbial communities. Microb. Ecol. 28, 237–243.
Suttle, C.A., Chen, F., 1992. Mechanisms and rates of decay of marine viruses in seawater. Appl. Environ. Microbiol. 58, 3721–3729.
Tazaki, K., 1994. Formation of fine-grained metal and silicate precipitates on a bacterial surface (*Bacillus subtilis*). Clays Clay Miner. 45, 203–212.
van der Wal, A., Norde, W., Zehnder, A.J.B., Lyklema, J., 1997. Determination of the total charge in the cell walls of gram-positive bacteria. Colloids Surf., B Biointerfaces 9, 81–100.
van Loosdrecht, M.C.M., Lyklema, J., Norde, W., Schraa, G., Zehnder, A.J.B., 1987. Electrophoretic mobility and hydrophobicity as a measure to predict the initial steps of bacterial adhesion. Appl. Environ. Microbiol. 53, 1898–1901.
Warren, L.A., Ferris, F.G., 1998. Continuum between sorption and precipitation of Fe(III) on microbial surfaces. Environ. Sci. Technol. 32, 2331–2337.
Wasserman, E., Felmy, A.R., 1998. Computation of the electrical double layer properties of semipermeable membranes in multicomponent electrolytes. Appl. Environ. Microbiol. 64, 2295–2300.
Weinbauer, M.G., Suttle, C., 1997. Comparison of epifluorescence and transmission electron microscopy for counting viruses in natural marine waters. Aquat. Microb. Ecol. 13, 225–232.
Wells, M.L., Goldberg, E.D., 1992. Marine submicron particles. Mar. Chem. 40, 5–18.
Wells, M.L., Goldberg, E.D., 1993. Colloid aggregation in seawater. Mar. Chem. 41, 353–358.
Wells, M.L., Goldberg, E.D., 1994. The distribution of colloids in the North Atlantic and Southern Oceans. Limnol. Oceanogr. 39, 286–302.
Westall, J.C., 1982. FITEQL: A computer program for the determination of chemical equilibrium constants from experimental data: Version 1.2, Report 82-01, Department of Chemistry, Oregon State University.

Wilhelm, S.W., Suttle, C.A., 1999. Viruses and nutrient cycles in the sea. Bioscience 49, 781–788.

Wommack, K.E., Colwell, R.R., 2000. Virioplankton: viruses in aquatic ecosystems. Microb. Molec. Biol. Rev. 64, 69–114.

Wonders, H.A.M., van Leeuwen, H.P., Lyklema, J., 1997. Metal- and proton-binding properties of a core-shell latex: interpretation in terms of colloid surface models. Colloids Surf., A Physicochem. Eng. Asp. 120, 221–233.

Wu, J., Luther III, G.W., 1994. Size-fractioned iron concentrations in the water column of the western North Atlantic Ocean. Limnol. Oceanogr. 39, 119–129.

Wu, J., Luther III, G.W., 1995. Complexation of Fe(III) by natural organic ligands in the Northwest Atlantic Ocean by a competitive ligand equilibration method and kinetic approach. Mar. Chem. 50, 159–177.

Wu, J., Luther III, G.W., 1996. Spatial and temporal distribution of iron in the surface water of the northwestern Atlantic Ocean. Geochim. Cosmochim. Acta 60, 2729–2741.

Wu, J., Boyle, E., Sunda, W., Wen, L.-S., 2001. Soluble and colloidal iron in the oligotrophic North Atlantic and North Pacific. Science 292, 847–849.

Wu, J., Sunda, W., Boyle, E.A., Karl, D.M., 2000. Phosphate depletion in the western North Atlantic Ocean. Science 289, 759–762.

Xue, H.-B., Stumm, W., Sigg, L., 1988. The binding of heavy metals to algal surfaces. Water Res. 22, 917–926.

Yee, N., Fein, J.B., 2001. Cd adsorption onto bacterial surfaces: a universal adsorption edge? Geochim. Cosmochim. Acta 65, 2037–2042.